Chinese Journal of Aeronautics, (2014),27(1): 59–64

Chinese Society of Aeronautics and Astronautics
& Beihang University

Chinese Journal of Aeronautics

cja@buaa.edu.cn
www.sciencedirect.com

Flutter analysis of an airfoil with nonlinear damping using equivalent linearization

Chen Feixin, Liu Jike, Chen Yanmao*

Department of Mechanics, Sun Yat-sen University, 510275 Guangzhou, China

Received 18 January 2013; revised 1 March 2013; accepted 29 May 2013
Available online 31 July 2013

KEYWORDS

Airfoil flutter;
Bifurcation;
Cubic damping;
Equivalent linearization;
Limit cycle oscillation

Abstract The equivalent linearization method (ELM) is modified to investigate the nonlinear flutter system of an airfoil with a cubic damping. After obtaining the linearization quantity of the cubic nonlinearity by the ELM, an equivalent system can be deduced and then investigated by linear flutter analysis methods. Different from the routine procedures of the ELM, the frequency rather than the amplitude of limit cycle oscillation (LCO) is chosen as an active increment to produce bifurcation charts. Numerical examples show that this modification makes the ELM much more efficient. Meanwhile, the LCOs obtained by the ELM are in good agreement with numerical solutions. The nonlinear damping can delay the occurrence of secondary bifurcation. On the other hand, it has marginal influence on bifurcation characteristics or LCOs.

1. Introduction

Nonlinear airfoil flutter is a typical self-excited vibration with rich nonlinear dynamical behaviors, such as limit cycle oscillation (LCO), bifurcation, and chaos.[1–4] Since not all the nonlinear features can be predicted by numerical methods, lots of analytic or semi-analytic techniques have been applied on airfoil models, for example, the harmonic balance method (HBM),[5,6] the incremental harmonic balance (IHB) method,[7,8] the perturbation-incremental method,[9] the homotopy analysis method,[10] and the equivalent linearization method (ELM),[11–14] to mention a few.

The ELM has been widely applied to various nonlinear vibration problems due to its simplicity and effectiveness. Furthermore, the approximate solution of the equivalent linear system has clear physical significance, which can provide us with convenience to analyze nonlinear dynamical behaviors. One of the most important procedures of the ELM is to derive an equivalent linear system by linearizing considered nonlinearities. Usually, the average method or the KBM method is employed for obtaining equivalent linear quantities.[3] Based on an equivalent linear system, methods for linear flutter analysis can be applied. For example, Liu and Zhao[1] gained the equivalent stiffness for cubic pitching nonlinearity by the average method. Later, Mickens[11] proposed a method by combining equivalent linearization and the averaging technique. Lim and Wu[12] combined the ELM and the HBM for solving strongly nonlinear vibration. Chen and Liu[13] improved the accuracy of equivalent stiffness by Lim's method to analyze the influences of quadratic pitching stiffness on a flutter system. Most recently, the ELM was extended to flutter systems with multiple nonlinearities, as suggested by Chen et al.[14]

* Corresponding author. Tel.: +86 20 84114211.
E-mail addresses: chenfeixin@hotmail.com (F. Chen), jikeliu@hotmail.com (J. Liu), chenyanmao@hotmail.com (Y. Chen).

Peer review under responsibility of Editorial Committee of CJA.

ELSEVIER Production and hosting by Elsevier

1000-9361 © 2014 Production and hosting by Elsevier Ltd. on behalf of CSAA & BUAA. Open access under CC BY-NC-ND license.
http://dx.doi.org/10.1016/j.cja.2013.07.020

Structural nonlinearities such as cubic pitch/plunge stiffness, freeplay, and hysteresis have been extensively investigated in nonlinear airfoil flutter. Nonlinear damping, however, has rarely been investigated. Note that nonlinear damping may arise in hinge moment, damper, or solid friction.[15–18] Nonlinear damping may also play a considerable part in the behavior of nonlinear systems, especially strongly coupled fluid–structure systems.[15] Via an experiment for tube arrays, Meskell and Fitzpatrick[16] pointed out that the resulted self-excited LCO amplitude was determined by nonlinear damping while linear damping dominated the instability flutter. After that, a method was suggested by Meskell[17] for estimating the damping parameters in lightly damped systems. The influences of damping on limit cycles were also described by Sinou and Jezequel.[18] To the best of our knowledge, very few investigations addressed the effect of nonlinear damping on airfoil flutter.

This study aims at extending the ELM to investigate the flutter system of an airfoil with structural nonlinear damping. Special emphasis is put on the effectiveness of the ELM and the influences of nonlinear damping on LCOs. The equivalent linearization quantity of nonlinear damping is obtained by the average method. The LCO frequency is chosen as an active increment to produce bifurcation charts. Then, the LCOs and bifurcation of the equivalent flutter system are analyzed in detail. Numerical examples validate the accuracy of the extended ELM.

2. Equations of motions

Fig. 1 shows the physical model of a two-dimensional airfoil, which oscillates in the pitch and plunge directions. The plunge deflection is denoted by $\bar{h}$, positive if downward; the symbol α denotes the pitch angle, positive if nose up. The length of the mid-chord is b. The mass center (c.g.) resides at a distance $x_\alpha b$ from the elastic axis (E). Besides, there is a distance $a_h b$ between the elastic axis and the mid-chord. The focal point F is the aerodynamic center. Both of the distances are positive when measured towards the trailing edge of the airfoil.

The coupled equations for the motions of the airfoil subject to subsonic aerodynamics can be modeled in a non-dimensional form as follows[4,19]

$$\begin{cases} \ddot{\xi}+x_\alpha\ddot{\alpha}+2\varsigma_\xi\overline{\omega}\dot{\xi}/U+(\overline{\omega}/U)^2G(\xi)=-C_L(t)/\pi\mu+P(t)b/mU^2 \\ x_\alpha\ddot{\xi}/r_\alpha^2+\ddot{\alpha}+2\varsigma_\alpha\dot{\alpha}/U+(1/U)^2M(\alpha)=2C_M(t)/\pi\mu r_\alpha^2+Q(t)b/mU^2r_\alpha^2 \end{cases} \tag{1}$$

where $\xi=\bar{h}/b$ is the non-dimensional displacement, and the prime denotes the differentiation with respect to the non-dimensional time t, which is defined as $t = Ut_1/b$ (t_1 is the real time and U is a non-dimensional flow velocity given by $U = V/b\omega_\alpha$ with V as the flow speed); $\overline{\omega}$ is indicated by $\overline{\omega}=\omega_\xi/\omega_\alpha$, where ω_ξ and ω_α are the uncoupled natural frequencies in the plunge and pitch modes, respectively; ς_ξ and ς_α are the damping ratios; $G(\xi)$ and $M(\alpha)$ denote the nonlinear terms of plunging and pitching, respectively; $P(t)$ and $Q(t)$ are the externally applied force and moment; r_α is the radius of gyration about the elastic axis; m is the airfoil mass per unit length while μ is the airfoil-air mass ratio. $C_L(t)$ and $C_M(t)$ denote the coefficients for lifting and moment, respectively. For an incompressible flow, $C_L(t)$ and $C_M(t)$ can be modeled by

$$\begin{cases} C_L(t)=\pi\left(\ddot{\xi}-a_h\ddot{\alpha}+\dot{\alpha}\right)+2\pi\left\{\alpha(0)+\dot{\xi}(0)+(1/2-a_h)\dot{\alpha}(0)\right\}\varphi(\tau) \\ \qquad +2\pi\int_0^t\varphi(t-\sigma)\left\{\dot{\alpha}(\sigma)+\ddot{\xi}(\sigma)+(1/2-a_h)\ddot{\alpha}(\sigma)\right\}\mathrm{d}\sigma \\ C_M(t)=\pi(1/2+a_h)\left\{\alpha(0)+\dot{\xi}(0)+(1/2-a_h)\dot{\alpha}(0)\right\}\varphi(\tau) \\ \qquad +\pi(1/2+a_h)\int_0^t\varphi(t-\sigma)\left\{\dot{\alpha}(\sigma)+\ddot{\xi}(\sigma)+(1/2-a_h)\ddot{\alpha}(\sigma)\right\}\mathrm{d}\sigma \\ \qquad +\pi a_h\left(\ddot{\xi}-a_h\ddot{\alpha}\right)/2-(1/2-a_h)\dfrac{\pi}{2}\dot{\alpha}-\pi\ddot{\alpha}/16 \end{cases} \tag{2}$$

where the Wagner function $\varphi(\tau)$ is given by the Jone's approximation $\varphi(t)=1-\psi_1\mathrm{e}^{-\varepsilon_1 t}-\psi_2\mathrm{e}^{-\varepsilon_2 t}$, with the constants $\psi_1 = 0.165$, $\psi_2 = 0.335$, $\varepsilon_1 = 0.0455$, and $\varepsilon_2 = 0.3$.[20]

Due to the existence of the integral terms in Eq. (2), Eq. (1) is a system of integro-differential equations. Studying the dynamic behavior of the system analytically can be rather cumbersome. Lee et al.[21] introduced four new variables for eliminating the integral terms

$$w_1=\int_0^t\mathrm{e}^{-\varepsilon_1(t-\sigma)}\alpha(\sigma)\mathrm{d}\sigma,\quad w_2=\int_0^t\mathrm{e}^{-\varepsilon_2(t-\sigma)}\alpha(\sigma)\mathrm{d}\sigma$$
$$w_3=\int_0^t\mathrm{e}^{-\varepsilon_1(t-\sigma)}\xi(\sigma)\mathrm{d}\sigma,\quad w_4=\int_0^t\mathrm{e}^{-\varepsilon_2(t-\sigma)}\xi(\sigma)\mathrm{d}\sigma$$

Thus, Eq. (1) can then be rewritten in a general form containing only differential operators as

$$\begin{cases} c_0\dddot{\xi}+c_1\ddot{\alpha}+c_2\ddot{\xi}+c_3\dot{\alpha}+c_4\xi+c_5\alpha+c_6w_1+c_7w_2 \\ \quad +c_8w_3+c_9w_4+c_{10}G(\xi)=f(t) \\ d_0\dddot{\xi}+d_1\ddot{\alpha}+d_2\ddot{\xi}+d_3\dot{\alpha}+d_4\xi+d_5\alpha+d_6w_1+d_7w_2+d_8w_3 \\ \quad +d_9w_4+d_{10}M(\alpha)=g(t) \end{cases} \tag{3}$$

where the coefficients $c_0, c_1, \cdots, c_{10}$ and $d_0, d_1, \cdots, d_{10}$ are given in Ref. 19. Both $f(t)$ and $g(t)$ depend on initial conditions, Wagner's function, and the external forcing terms,

$$\begin{cases} f(t)=\frac{2}{\mu}\left\{\left(\frac{1}{2}-a_h\right)\alpha(0)+\xi(0)\right\}(\psi_1\varepsilon_1\mathrm{e}^{-\varepsilon_1 t}+\psi_2\varepsilon_2\mathrm{e}^{-\varepsilon_2 t})+\dfrac{P(t)b}{mU^2} \\ g(t)=-\dfrac{1+2a_h}{2r_\alpha^2}f(t)+\dfrac{Q(t)}{mU^2r_\alpha^2} \end{cases}$$

Generally, the identification of the nonlinearities on the airfoil is very complicated. The nonlinear damping terms are usually assumed to be proportional to the cubic power of velocity.[22] In this study, we consider the system with cubic damping as

$$\begin{cases} G(\xi)=k_\xi\xi+e_\xi\dot{\xi}^3 \\ M(\alpha)=k_\alpha\alpha+e_\alpha\dot{\alpha}^3 \end{cases} \tag{4}$$

where k_ξ, k_α, e_ξ and e_α are all constants.

Introduce a variable vector $\boldsymbol{X}=[x_1 \quad x_2 \quad \cdots \quad x_8]^{\mathrm{T}}$ with $x_1=\alpha$, $x_2=\dot{\alpha}$, $x_3=\xi$, $x_4=\dot{\xi}$, $x_5=w_1$, $x_6=w_2$, $x_7=w_3$

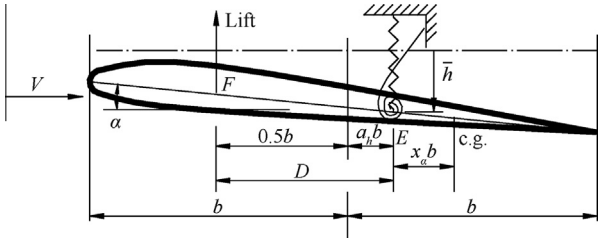

Fig. 1 Physical model of a two-dimensional airfoil.

and $x_8 = w_4$. Assume there is no external forcing, i.e., $P(t) = Q(t) = 0$ in Eq. (1). For large values of t, when the system exhibits a steady motion, we can let $f(t) = g(t) = 0$. Then, Eq. (3) can be written as a set of eight first-order ordinary differential equations (ODEs) described in a vector form

$$\dot{\boldsymbol{X}} = \boldsymbol{L}(U)\boldsymbol{X} + \boldsymbol{N}(\boldsymbol{X}, U) \tag{5}$$

where $\boldsymbol{L}(U)$and $\boldsymbol{N}(\boldsymbol{X}, U)$ are the coefficient matrix for the linear and nonlinear parts, respectively. As a result of this reduced-order method, the numerical computation can now be applied in analyzing the original aeroelastic system. For more details of system Eq. (5), please refer to Ref. [19] or Ref. [21]

3. ELM

In the ELM, the equivalent linear quantities by the average method can be expressed as

$$k_{\text{eq}} = -\frac{1}{\pi A}\int_0^{2\pi} f(A\cos\varphi, -A\omega\sin\varphi)\cos\varphi \mathrm{d}\varphi \tag{6}$$

$$c_{\text{eq}} = \frac{1}{\pi A\omega}\int_0^{2\pi} f(A\cos\varphi, -A\omega\sin\varphi)\sin\varphi \mathrm{d}\varphi \tag{7}$$

where ω is the LCO frequency corresponding to the wind speed, A denotes the complex amplitudes of pitch.

Considering the nonlinear terms as Eq. (4), we can deduce the equivalent linear quantities for cubic nonlinear damping according to Eqs. (6) and (7) as follows

$$\begin{cases} c_{\xi\text{eq}} = q_1 e_\xi H^2\omega^2, & k_{\xi\text{eq}} = k_\xi \\ c_{\alpha\text{eq}} = q_2 e_\alpha A^2\omega^2, & k_{\alpha\text{eq}} = k_\alpha \end{cases} \tag{8}$$

where q_1 and q_2 are constants, the values of which are usually chosen as $q_1 = q_2 = 3/4$, H denotes the complex amplitudes of plunge.

Substitution of Eq. (8) into Eq. (4) results in

$$\begin{cases} G(\xi) = k_\xi\xi + c_{\xi\text{eq}}\dot{\xi} \\ M(\alpha) = k_\alpha\alpha + c_{\alpha\text{eq}}\dot{\alpha} \end{cases} \tag{9}$$

Substituting Eq. (9) in Eq. (3), the equivalent linear equations can be given as

$$\begin{cases} c_0\ddot{\xi} + c_1\ddot{\alpha} + (c_2 + c_{10}c_{\xi eq})\dot{\xi} + c_3\dot{\alpha} + (c_4 + c_{10}k_\xi)\xi + c_5\alpha + c_6 w_1 \\ \quad + c_7 w_2 + c_8 w_3 + c_9 w_4 = 0 \\ d_0\ddot{\xi} + d_1\ddot{\alpha} + d_2\dot{\xi} + (d_3 + d_{10}c_{\alpha eq})\dot{\alpha} + d_4\xi + (d_5 + d_{10}k_\alpha)\alpha \\ \quad + d_6 w_1 + d_7 w_2 + d_8 w_3 + d_9 w_4 = 0 \end{cases} \tag{10}$$

Under the assumption of harmonic motion, the LCO amplitude can be expressed by

$$\begin{cases} \xi = H\mathrm{e}^{\mathrm{i}\omega t} \\ \alpha = A\mathrm{e}^{\mathrm{i}\omega t} \end{cases} \tag{11}$$

Substituting Eq. (11) into Eq. (10), one can obtain the flutter determinant

$$\begin{vmatrix} C_1 & C_2 \\ C_3 & C_4 \end{vmatrix} = 0 \tag{12}$$

where

$$\begin{cases} C_1 = -c_0\omega^2 + (c_4 + c_{10}k_\xi) + c_8/(\varepsilon_1 + \omega\mathrm{i}) + c_9/(\varepsilon_2 + \omega\mathrm{i}) \\ \quad + (c_2 + c_{10}c_{\xi\text{eq}})\omega\mathrm{i} \\ C_2 = -d_0\omega^2 + d_4 + d_8/(\varepsilon_1 + \omega i) + d_9/(\varepsilon_2 + \omega\mathrm{i}) + d_2\omega\mathrm{i} \\ C_3 = -c_1\omega^2 + c_5 + c_6/(\varepsilon_1 + \omega\mathrm{i}) + c_7/(\varepsilon_2 + \omega\mathrm{i}) + c_3\omega\mathrm{i} \\ C_4 = -d_1\omega^2 + (d_5 + d_{10}k_a) + d_6/(\varepsilon_1 + \omega\mathrm{i}) + d_7/(\varepsilon_2 + \omega\mathrm{i}) \\ \quad + (d_3 + d_{10}c_{\alpha\text{eq}})\omega\mathrm{i} \end{cases}$$

Separating the imaginary and real parts of Eq. (12), for $\omega \neq 0$, we can deduce the following equations:

$$\begin{aligned} &\left[c_4 + c_{10}k_\xi - c_0\omega^2 + c_8\varepsilon_1/\left(\varepsilon_1^2 + \omega^2\right) + c_9\varepsilon_2/\left(\varepsilon_2^2 + \omega^2\right)\right] \\ &\quad\times\left[d_5 + d_{10}k_a - d_1\omega^2 + d_6\varepsilon_1/\left(\varepsilon_1^2 + \omega^2\right) + d_7\varepsilon_2/\left(\varepsilon_2^2 + \omega^2\right)\right] \\ &\quad-\left[c_2\omega - c_8\omega/\left(\varepsilon_1^2 + \omega^2\right) - c_9\omega)/\left(\varepsilon_2^2 + \omega^2\right) + c_{10}c_{\xi\text{eq}}\omega\right] \\ &\quad\times\left[d_3\omega - d_6\omega/\left(\varepsilon_1^2 + \omega^2\right) - d_7\omega/\left(\varepsilon_2^2 + \omega^2\right) + d_{10}c_{\alpha\text{eq}}\omega\right] \\ &\quad-\left[c_5 - c_1\omega^2 + c_6\varepsilon_1/\left(\varepsilon_1^2 + \omega^2\right) + c_7\varepsilon_2/\left(\varepsilon_2^2 + \omega^2\right)\right] \\ &\quad\times\left[d_4 - d_0\omega^2 + d_8\varepsilon_1/\left(\varepsilon_1^2 + \omega^2\right) + d_9\varepsilon_2/\left(\varepsilon_2^2 + \omega^2\right)\right] \\ &\quad+\left[c_6\omega/\left(\varepsilon_1^2 + \omega^2\right) - c_3\omega + c_7\omega/\left(\varepsilon_2^2 + \omega^2\right)\right] \\ &\quad\times\left[d_8\varepsilon_1/\left(\varepsilon_1^2 + \omega^2\right) - d_2\omega + d_9\omega/\left(\varepsilon_2^2 + \omega^2\right)\right] = 0 \end{aligned} \tag{13}$$

$$\begin{aligned} &\left[d_3 - d_6/\left(\varepsilon_1^2 + \omega^2\right) - d_7/\left(\varepsilon_2^2 + \omega^2\right) + d_{10}c_{\alpha\text{eq}}\right] \\ &\quad\times\left[c_4 + c_{10}k_\xi - c_0\omega^2 + c_8\varepsilon_1/\left(\varepsilon_1^2 + \omega^2\right) + c_9\varepsilon_2/\left(\varepsilon_2^2 + \omega^2\right)\right] \\ &\quad+\left[c_2 - c_8/\left(\varepsilon_1^2 + \omega^2\right) - c_9/\left(\varepsilon_2^2 + \omega^2\right) + c_{10}c_{\xi\text{eq}}\right] \\ &\quad\times\left[d_5 + d_{10}k_a - d_1\omega^2 + d_6\varepsilon_1/\left(\varepsilon_1^2 + \omega^2\right) + d_7\varepsilon_2/\left(\varepsilon_2^2 + \omega^2\right)\right] \\ &\quad+\left[d_8/\left(\varepsilon_1^2 + \omega^2\right) - d_2 + d_9/\left(\varepsilon_2^2 + \omega^2\right)\right] \\ &\quad\times\left[c_5 - c_1\omega^2 + c_6\varepsilon_1/\left(\varepsilon_1^2 + \omega^2\right) + c_7\varepsilon_2/\left(\varepsilon_2^2 + \omega^2\right)\right] \\ &\quad+\left[c_6/\left(\varepsilon_1^2 + \omega^2\right) - c_3 + c_7/\left(\varepsilon_2^2 + \omega^2\right)\right] \\ &\quad\times\left[d_4 - d_0\omega^2 + d_8\varepsilon_1/\left(\varepsilon_1^2 + \omega^2\right) + d_9\varepsilon_2/\left(\varepsilon_2^2 + \omega^2\right)\right] = 0 \end{aligned} \tag{14}$$

$$\frac{H}{A} = \frac{c_0\omega^2 - (c_4 + c_{10}k_\xi) - c_8/(\varepsilon_1 + \omega\mathrm{i}) - c_9/(\varepsilon_2 + \omega\mathrm{i}) - (c_2 + c_{10}c_{\xi\text{eq}})\omega\mathrm{i}}{-c_1\omega^2 + c_5 + c_6/(\varepsilon_1 + \omega\mathrm{i}) + c_7/(\varepsilon_2 + \omega\mathrm{i}) + c_3\omega\mathrm{i}} \tag{15}$$

The flutter velocity, frequency, and amplitude can be determined by solving Eqs. (8), (13)–(15). As there are 6 unknowns in 5 equations, the equations are indeterminate. In order to determine the solutions, we can implement the routine procedures of the ELM.

Step 1 Assume A as a positive constant, and then set the non-dimensional flow velocity U and the LCO frequency ω as variables. Eq. (15) describes the relation between A and H.

Step 2 Combining Eqs. (8), (13), and (14), one can obtain a group of ω corresponding to one value of A. Choose the real value of ω as the appropriate frequency.

Step 3 Solving U by substituting the real value of ω and A into Eq. (13). Thus, the curve of U versus A can be drawn.

This approach is employed routinely in producing bifurcation charts by ELM. However, one problem of the above procedures is that it will cost many computational resources on filtering the correct frequency from various results in Step 2. Here, we present a modified approach as follows:

Step 1 Assume the frequency ω as a positive constant, and then set U and A as variables.
Step 2 Substituting Eq. (8) into Eqs. (13) and (14), the algebraic equations about U and A can be deduced.
Step 3 Solving these equations, one can obtain the relation between U and A.

The bifurcation charts can be drawn through one of the above approaches. Compared with the first one, the second approach can avoid the filtering process of various approximations for frequency. The efficiencies of the two solution approaches will be examined.

4. Numerical examples

In this section, the numerical solutions obtained by the Runge–Kutta method will be used to validate the ELM results. The system parameters under consideration are $\mu = 100$, $r_\alpha = 0.5$, $a_h = -0.5$, $\varsigma_\alpha = \varsigma_\xi = 0$, $\overline{\omega} = 0.25$, $x_\alpha = 0.25$, and the value of U varies.

Example I $k_\xi = k_\alpha = 1$, $e_\xi = 0$, $e_\alpha = 80$.

As one can see in Fig. 2, there is a subcritical Hopf bifurcation on the critical flutter speed ($U_f = 6.0385$). Two LCOs arise before U_f. The upper one is stable and the other is unstable. Intuitively, an LC is considered as stable as it can be tracked by time-marching integration. Otherwise, it is unstable. As q_2 is chosen as 0.75, the stable LCOs obtained by ELM approximate the numerical ones with a relative error below 15%. The unstable results from ELM are in nice agreement with the solutions obtained by the IHB method with 9 harmonics. Fig. 3 shows the LCO frequency from ELM agrees well with the numerical results. As U increases, the frequency of stable LCO reduces while that of unstable LCO increases. It should be pointed out that, although the ELM is not appealing in quantitative analysis for this case, it can track the main characteristics of the bifurcations. The reason for the low accuracy will be analyzed by comparing with another example.

The validity and efficiency are analyzed for the above two approaches when applied to draw bifurcation charts. According to Fig. 4, the solutions provided by the two approaches (the first one by assuming A as an active increment, the second one by assuming ω as an active increment) are consistent with each other. Table 1 shows that the modified approach (the second one) is much more efficient than the first one. Compared with the modified approach, the first method spends much more computational resources on properly selecting approximate solutions. Therefore, the original ELM needs much more runtime.

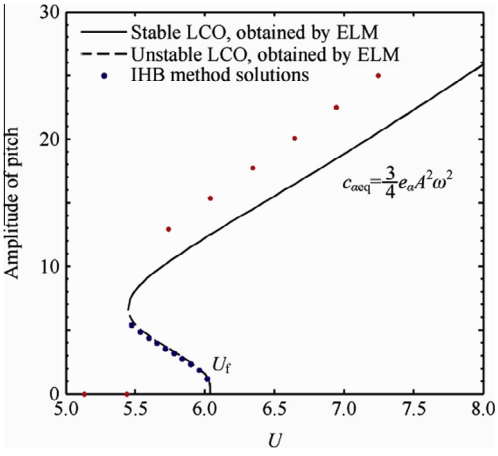

Fig. 2 Comparison of LCO amplitudes for Example I.

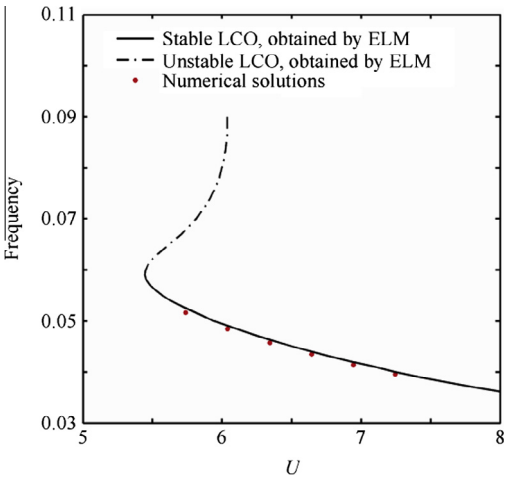

Fig. 3 Comparison of LCO frequency for Example I.

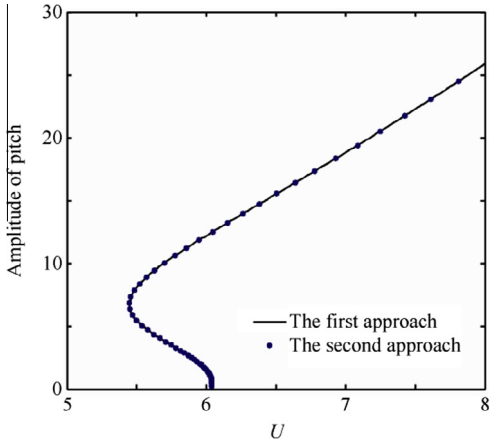

Fig. 4 Bifurcation charts provided by the two different approaches for Example I.

Table 1 Comparison of computational time spent on drawing the bifurcation chart by employing the two approaches, respectively.

Parameter	The first approach	The second approach
Active increment region	A = [0:30]	ω = [0.09:0.03]
Step size	0.5	0.001
Runtime (s)	158.8	6.232
Calculation points	61	61

Example II $k_\xi = k_\alpha = 1$, $e_\xi = 80$, $e_\alpha = 0$.

In this example, we consider cubic plunging damping by choosing $e_\xi = 80$. Fig. 5 shows the curve of U–H with $c_{\xi eq} = \frac{3}{4}e_\xi H^2\omega^2$. Note that, in this case, very good agreement

can be observed between the ELM results and the numerical ones. The critical flutter wind speed can be found at $U_f = 6.0385$. In addition, a subcritical Hopf bifurcation arises at the critical point. A turning point occurs at $U_C = 5.780$ or so, at which the unstable LCO gains its stability. The frequencies provided by the ELM are shown in Fig. 6. They agree well with the numerical ones. Both Figs. 5 and 6 can validate the ELM.

It is worthy of pointing out that the ELM provides much more accurate approximations for Example II than for Example I. According to Eq. (11), in the solution process of the ELM, the LCOs of the airfoil are assumed to be harmonic. Therefore, the accuracy for the ELM depends on how closely the LCOs approach harmonic motions. Fig. 7 shows the phase planes of LCOs for both of the two examples obtained by numerical solutions and ELM, respectively. For Example I, there is a great difference between the true LCO and the ELM solution. Note that the ELM approximation is harmonic no matter it is accurate or not. As for Example II the true LCO can be roughly considered as harmonic.

In order to evaluate the influence of cubic nonlinear damping on the airfoil motions, both cubic damping and stiffness are applied to the origin nonlinear system (3), i.e., $M(\alpha) = \alpha + 80\dot{\alpha}^3 + 80\alpha^3$. According to Fig. 8, the difference caused by nonlinear damping occurs only at the secondary bifurcation. The appearance of the secondary bifurcation is delayed. Note that the ELM is incapable of tracking the secondary bifurcation at its present state. Fig. 9 presents a typical case representing supercritical Hopf bifurcation obtained by ELM and the numerical example, respectively. When cubic nonlinear stiffness and damping are adopted simultaneously, the system preserves the profile of the bifurcations. The first bifurcation appears as a supercritical Hopf bifurcation.

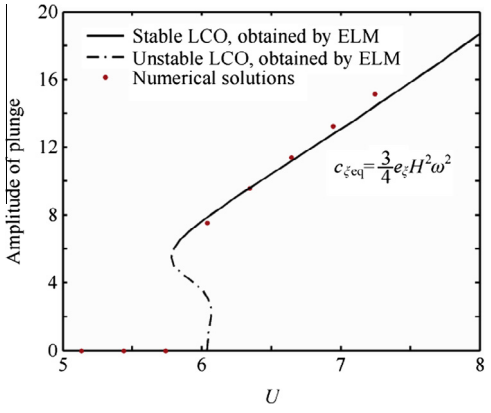

Fig. 5 Comparison of LCO amplitudes for Example II.

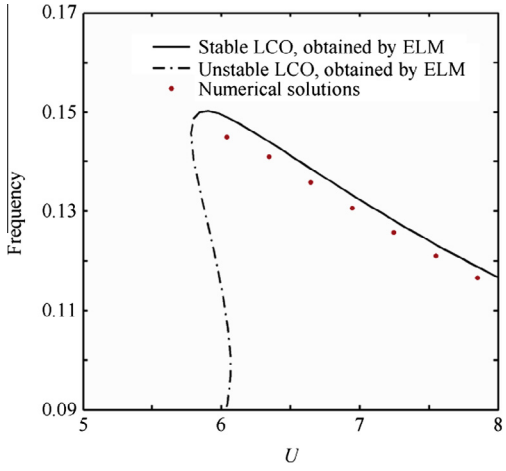

Fig. 6 Comparison of LCO frequencies for Example II.

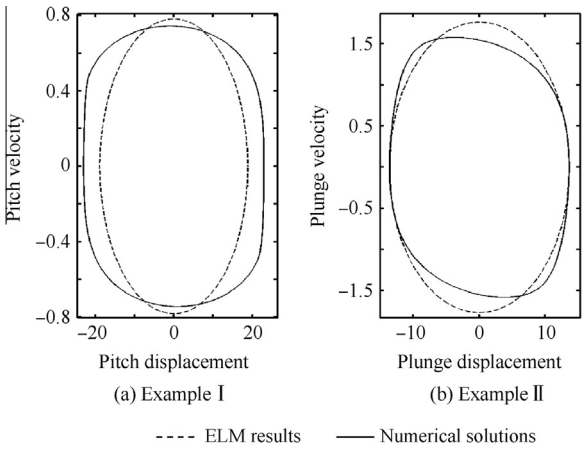

Fig. 7 Comparisons of LCOs' phase plane obtained by ELM and by numerical methods with $U = 7$.

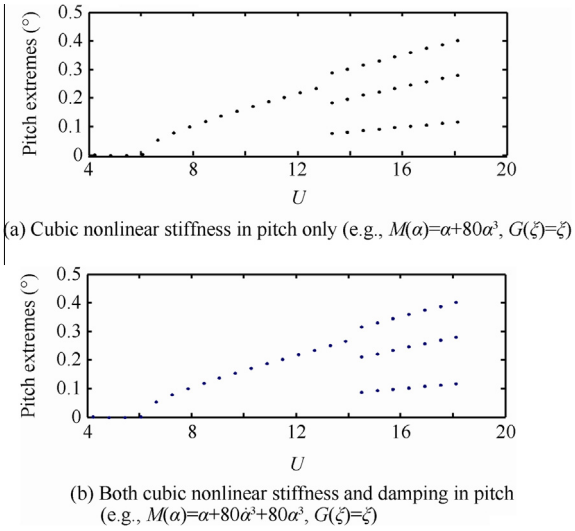

Fig. 8 Bifurcations for the flutter system with different nonlinear terms obtained by numerical example.

5. Conclusion

The ELM has been modified, via incrementing the LCO frequency, to analyze the bifurcation of the airfoil flutter system with nonlinear damping. Numerical examples show that the LCO amplitudes and frequencies can be obtained approximately by the modified ELM. Furthermore, it is much more efficient to track the bifurcation charts by using the modified approach than by the routinely used procedures. The modified approach could be applicable in more nonlinear systems, especially those with nonlinear damping.

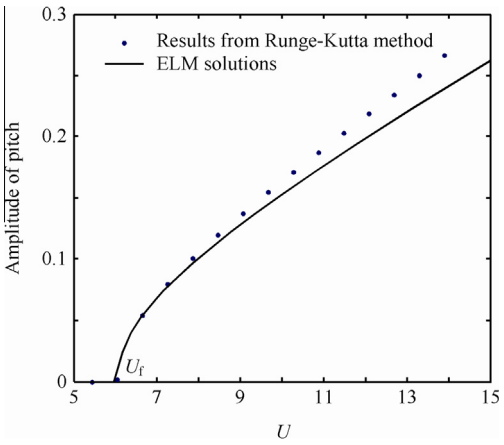

Fig. 9 The first bifurcation of the system including both cubic nonlinear stiffness and damping in pitch (e.g., $M(\alpha) = \alpha + 80\dot{\alpha}^3 + 80\alpha^3$, $G(\xi) = \xi$).

Acknowledgment

This work was supported by the National Natural Science Foundation of China (Nos.: 11002088, 11172333, 11272361).

References

1. Liu JK, Zhao LC. Bifurcation analysis of airfoils in incompressible flow. *J Sound Vib* 1992;**154**(1):117–24.
2. Zhang J, Xiang JW. Nonlinear aeroelastic response of high-aspect-ratio flexible wings. *Chin J Aeronaut* 2009;**22**(4):355–63.
3. Lee BHK, Price SJ, Wong YS. Nonlinear aeroelastic analysis of airfoils: bifurcation and chaos. *Prog Aerosp Sci* 1999;**35**(3):205–334.
4. Liu L, Dowell EH, Thomas JP. A high dimensional harmonic balance approach for an aeroelastic airfoil with cubic restoring forces. *J Fluids Struct* 2007;**23**(3):351–63.
5. Cooper K, Mickens RE. Generalized harmonic balance/numerical method for determining analytical approximations to the periodic solutions of the $x(4/3)$ potential. *J Sound Vib* 2002;**250**(5):951–4.
6. Irani S, Sarrafzadeh H, Amoozgar MR. Bifurcation in a 3-DOF airfoil with cubic structural nonlinearity. *Chin J Aeronaut* 2011;**24**(3):265–78.
7. Raghothama A, Narayanan S. Non-linear dynamics of a two-dimensional airfoil by incremental harmonic balance method. *J Sound Vib* 1999;**226**(3):493–517.
8. Chen YM, Liu JK, Meng G. Incremental harmonic balance method for nonlinear flutter of an airfoil with uncertain-but-bounded parameters. *Appl Math Model* 2012;**36**(2):657–67.
9. Cao YY, Chung KW, Xu J. A novel construction of homoclinic and heteroclinic orbits in nonlinear oscillators by a perturbation-incremental method. *Nonlinear Dyn* 2011;**64**(3):221–36.
10. Chen YM, Liu JK, Meng G. Relationship between the homotopy analysis method and harmonic balance method. *Commun Nonlinear Sci Num Simul* 2010;**15**(8):2017–25.
11. Mickens RE. A combined equivalent linearization and averaging perturbation method for non-linear oscillator equations. *J Sound Vib* 2003;**264**(5):1195–200.
12. Lim CW, Wu BS. A new analytical approach to the Duffing-harmonic oscillator. *Phys Lett A* 2003;**311**(4–5):365–73.
13. Chen YM, Liu JK. On the limit cycles of aeroelastic systems with quadratic nonlinearities. *Struct Eng Mech* 2008;**30**(1):67–76.
14. Chen FX, Chen YM, Liu JK. Equivalent linearization method for the flutter system of an airfoil with multiple nonlinearities. *Commun Nonlinear Sci Num Simul* 2012;**17**(12):4529–35.
15. Crandall S. The role of damping in vibration theory. *J Sound Vib* 1970;**11**(1):3-IN1.
16. Meskell C, Fitzpatrick JA. Investigation of the nonlinear behaviour of damping controlled fluidelastic instability in a normal triangular tube array. *J Fluids Struct* 2003;**18**(5):573–93.
17. Meskell C. A decrement method for quantifying nonlinear and linear damping parameters. *J Sound Vib* 2006;**296**(3):643–9.
18. Sinou JJ, Jezequel L. The influence of damping on the limit cycles for a self-exciting mechanism. *J Sound Vib* 2007;**304**(3–5):875–93.
19. Liu LP, Dowell EH. The secondary bifurcation of an aeroelastic airfoil motion: effect of high harmonics. *Nonlinear Dyn* 2004;**37**(1):31–49.
20. Jones RT. *The unsteady lift of a wing of finite aspect ratio*; 1940. Report No: NACA, Report 681.
21. Lee B, Gong L, Wong Y. Analysis and computation of nonlinear dynamic response of a two-degree-of-freedom system and its application in aeroelasticity. *J Fluids Struct* 1997;**11**(3):225–46.
22. Trueba JL, Rams J, Sanjuan AF. Analytical estimates of the effect of nonlinear damping in some nonlinear oscillators. *Int J Bifurcation Chaos* 2000;**10**(9):2257–67.

Chen Feixin is a Ph.D. student at the Department of Mechanics, Sun Yat-sen University. She received the B.S. degree from the same university in 2006. Her area of research includes nonlinear vibration and its application.

Liu Jike is a professor in the Department of Mechanics, Sun Yat-sen University. His current research interests are analysis methods of engineering structures, nonlinear vibration and fluid-structure interaction mechanics.

Chen Yanmao received his bachelor's degree in applied mathematics from Yichun College in 2004. He received his doctor's degree in mechanics from Sun Yat-sen University in 2009. From 2009 to 2011, he was a postdoc in the Institute of Mechanical Engineering at Shanghai Jiaotong University. In April 2011, he joined Sun Yat-sen University, and is now an associate professor in the Department of Mechanics. His research focused on nonlinear dynamics, flutter problems in aircraft and mechanical engineering, etc.